Research Square

Preprints are preliminary reports that have not undergone peer review.
They should not be considered conclusive, used to inform clinical practice,
or referenced by the media as validated information.

Direct utilization of long-chain fatty acid for methane production by thermophilic Archaeoglobi

Fengping Wang

fengpingw@sjtu.edu.cn

Shanghai Jiao Tong University https://orcid.org/0000-0002-3429-8410

Tiantian Yu

Shanghai Jiao Tong University https://orcid.org/0000-0003-3257-612X

Shujian Yuan

Shanghai Jiao Tong University

Yinzhao Wang

State Key Laboratory of Microbial Metabolism, School of Life Science and Biotechnology, Shanghai Jiao Tong University https://orcid.org/0000-0001-8715-1386

Article

Keywords:

Posted Date: October 24th, 2025

DOI: https://doi.org/10.21203/rs.3.rs-7873196/v1

License: This work is licensed under a Creative Commons Attribution 4.0 International License.
Read Full License

Additional Declarations: There is **NO** Competing Interest.

Version of Record: A version of this preprint was published at Nature Microbiology on September 15th, 2026. See the published version at https://doi.org/10.1038/s41564-026-02490-5.

Direct utilization of long-chain fatty acid for methane production by thermophilic *Archaeoglobi*

Tiantian Yu[1]*, Shujian Yuan[1], Yinzhao Wang[2], Fengping Wang[1]*

[1] State Key Laboratory of Submarine Geoscience; Key Laboratory of Polar Ecosystem and Climate Change, Ministry of Education; Shanghai Key Laboratory of Polar Life and Environment Sciences; and School of Oceanography, Shanghai Jiao Tong University, Shanghai, China;

[2] State Key Laboratory of Microbial Metabolism, School of Life Sciences and Biotechnology, Shanghai Jiao Tong University, 200240 Shanghai, China.

*To whom correspondence should be addressed. E-mail: fengpingw@sjtu.edu.cn; yutiantian@sjtu.edu.cn.

Abstract

The methanogenic degradation of long-chain fatty acids has traditionally been considered to occur through syntrophic partnerships between long-chain fatty acid degrading bacteria and methanogenic archaea. However, recent genomic evidence suggests that certain archaea may independently perform entire process. Here, we report the cultivation of an archaeon from the class *Archaeoglobi*, *Candidatus* (*Ca.*) Methanoglobus sphaerolipidus DLY3, from hot spring sediments in Tengchong, China. Using an integrated approach including targeted cultivation, growth experiments, microscopy, stable isotope tracing, metagenomics, and metatranscriptomics, we demonstrate that *Ca.* M. sphaerolipidus directly converts long-chain fatty acids to methane. This transformation involves the beta-oxidation pathway, the Wood-Ljungdahl pathway (WLP), and methanogenic methyl-coenzyme M reductase (MCR) and methyltransferases (MTR) complexes—a process we term liparotrophy. In addition to oleic acid, *Ca.* M. sphaerolipidus is also capable of utilizing methanol as a substrate for methanogenesis. Our findings expand the known substrate range for methanogenic archaea beyond CO_2 reduction, acetoclastic methanogenesis, methylotrophy, methyl reduction, methoxydotrophy, and the recently reported alkylotrophy.

Introduction

Methanogens are strictly anaerobic archaea that conserve energy through methane production and are responsible for approximately two-thirds of global methane emissions (576 Tg per year)[1, 2]. Traditionally, methanogenesis has been classified into five pathways based on substrate utilization: hydrogenotrophic (using CO_2 + H_2), acetoclastic (using acetate), methylotrophic (using methanol, methylamines, methyl sulfides), methyl reduction (using H_2 + methanol/methylamines), methoxydotrophic (using methoxylated aromatic compounds)[3, 4]. The recent discovery of a sixth pathway, alkylotrophy, in which *Ca.* Methanoliparia metabolizes long-chain alkanes to methane, revealed a broader range of natural substrates than previously recognized[5].

Methanogens were long believed to be exclusive to the *Euryarchaeota* superphylum. However, the recent successful cultivation of methanogenic lineages within the TACK superphylum—including phylum *Korarchaeota* and *Thermoproteota* (*Methanomethylicales* and *Nezhaarchaeales*)—has experimentally validated methanogenesis beyond *Euryarchaeota*[6-9].

All known methanogenic pathways converge at the final step of methane formation, catalyzed by the MCR complex. MCR also catalyzes the reverse reaction during anaerobic methane oxidation[10]. The analogous of MCR, alkyl-CoM reductases (ACRs), activate multi-carbon alkanes, enabling their anaerobic degradation[5, 11-15]. Phylogenetic analysis of McrA and AcrA sequences identifies three major clades: the conventional MCR clade, the TACK clade, and the ACR clade[16, 17]. Most sequences within the TACK clade originate from *Thermoproteota* and are implicated in methanogenesis[16, 17].

Even within traditional *Euryarchaeota* groups, methanogenic activity has been reported in lineages previously considered non-methanogenic[18-21]. Recently, an enrichment culture of *Ca.* Methanoglobus hypatiae LCB24—a methanogen from the *Archaeoglobaceae* family (class *Archaeoglobi*) isolated from a Yellowstone National Park hot spring—was shown to produce methane from mono-, di-, and trimethylamine[18]. Multiple genomes within the genus *Ca.* Methanoglobus encode MCR [18-21]. Unlike other euryarchaeotal methanogens, the McrA of *Ca.* Methanoglobus cluster within the TACK superphylum, suggesting acquisition via horizontal gene transfer[16-18, 21]. Additionally, genomes from the family JdFR-42 (class Archaeoglobi) contain alkyl-ACR genes[21], indicating potential for anaerobic alkane degradation. Notably, *mcr*-carrying *Ca.* Methanoglobus genomes are frequently detected in terrestrial hot

springs[18-21], whereas *acr*-encoding JdFR-42 genomes have been reported in marine environments[21].

Besides methylotrophic methanogenesis, members of *Ca.* Methanoglobus possess a complete beta-oxidation pathway[18]. Similarly, the long-chain alkane-degrading methanogen *Ca.* Methanoliparia also contains a complete beta-oxidation pathway[5]. The beta-oxidation pathway mediates long-chain fatty acid degradation by progressively cleaving two-carbon units from the carboxyl terminus to generate acetyl-CoA. Notably, the genomes of these archaea concomitantly encode the complete WLP and key enzymes essential for methanogenesis, including MTR and MCR [5, 18]. Through the coordinated actions of the WLP, MTR, and MCR, the acetyl-CoA generated via beta-oxidation can be converted to methane and carbon dioxide. Based on these genomic features, we hypothesized that these archaea might utilize long-chain fatty acids as a substrate for methanogenesis. Here, we report the cultivation of *Ca.* M. sphaerolipidus DLY3 from Tengchong hot spring sediments. Using integrated approaches, we demonstrate that *Ca.* M. sphaerolipidus directly converts long-chain fatty acids to methane.

Results and Discussion

Cultivation

After inoculating hot spring sediment into culture medium supplemented with 500 μL of oleic acid (Fig. S1), pronounced methane production was observed during the initial 100 days incubation (Fig. 1a, Supplementary Table 1). On day 106, the headspace of each bottle was replaced with N_2 to prevent excessive pressure buildup. Methane production continued from day 106 to day 129. Methane accumulation rates decreased between days 129 and 150. On day 156, an additional 200 μL of oleic acid was added, and the headspace was again flushed with N_2. Methanogenesis persisted throughout extended incubation. In contrast, only trace methane was detected in the control groups without oleic acid. On day 238, cultures were collected for metagenomic sequencing.

Through metagenomic sequencing, we reconstructed six high-quality metagenome-assembled genomes (MAGs) of the genus *Ca.* Methanoglobus (WYZ-LMO2, class *Archaeoglobi*, phylum *Halobacteriota* according to GTDB), designated *Ca.* M. sphaerolipidus DLY3, with 92.16-99.35% completeness and 1.63% contamination (Supplementary Table 2). *Ca.* M. sphaerolipidus was highly enriched in the oleic acid-amended cultures, with relative abundances of 69.9% and 74.2% (Fig.

1b). No sequences from this genus were detected in the original sediment[15], before incubation sample, and oleic acid-free controls. Based on average amino acid identity (AAI/ANI), *Ca.* M. sphaerolipidus genome was most closely related to MAGs GMQP_D_bin_18, JZ-3_D_bin_138, HHBFW-2_201803_bins_10, and JZ-3_201705_bins_59 (ANI 98.33–99.01%, AAI 98.33–98.91%) (Fig. S2, Supplementary Table 3), which were also obtained from Tengchong hot springs. Observations of the enrichment culture via hybridization chain reaction-fluorescence in situ hybridization (HCR-FISH) and scanning electron microscopy (SEM) showed that most cells exhibited a regular to irregular coccoid morphology, with widths ranging from 0.5 to 1 μm (Fig. 1c, d). This morphological characteristic is consistent with previous descriptions of other species in the archaeal class *Archaeoglobi*[18, 22, 23].

Methane production from oleic acid

Following the addition of 100 μL of oleic acid (Fig. S1), sustained production of methane and carbon dioxide was detected by day 27 (Fig. 2a, Supplementary Table 1). Production rates decreased between days 27 and 33. By day 33, methane and carbon dioxide levels reached 2166–3169 μmol and 954–1455 μmol, respectively. Subsequently, the ^{13}C-labeled oleic acid was added, ^{13}C-CH_4 and ^{13}C-CO_2 production was detected, reaching 171–203 μmol and 93–95 μmol at day 33, respectively.

Metagenomic and metatranscriptomic analyses confirmed *Ca.* M. sphaerolipidus as the dominant taxon, with relative abundances of 79.1% and 74.2% in the metagenomes, and 87.3% and 82.8% in the metatranscriptomes, respectively (Fig. 2b). Other MAGs included *Pseudothermotoga* and *Thermodesulfovibrio*, with genomic abundances below 13.5% and transcriptomic abundances below 6.5%. Low-abundance methanogenic archaeal MAGs were also detected, with genomic abundance <3.8% and transcriptomic abundance <1.0%.

Methane production from methanol

After adding 72.9 μL of methanol (Fig. S1), sustained methane and carbon dioxide production was detected till day 27 (Fig. 3a, Supplementary Table 1). Production ceased between days 27 and 30. By day 27, methane and carbon dioxide levels were 1224–1325 μmol and 576–646 μmol, respectively. With ^{13}C-labeled methanol, ^{13}C-CH_4 and ^{13}C-CO_2 production reached 115–117 μmol and 48–49 μmol by day 27, respectively.

Metagenomic and metatranscriptomic sequencing confirmed *Ca.* M. sphaerolipidus as the dominant taxon, with relative abundances of 76.3% and 81.0% in the metagenomes, and 93.4% and 95.4% in the metatranscriptomes, respectively (Fig.

3b). Trace amounts of bacteria and other methanogenic archaea were detected in both the metagenome and metatranscriptome, with abundances below 4%.

The pathway of methane production from oleic acid

The beta-oxidation pathway is recognized to mediate long-chain fatty acid degradation through sequential cleavage of two-carbon units from the carboxyl terminus, yielding acetyl-CoA. Metagenomic and metatranscriptomic analyses confirm that the *Ca.* M. sphaerolipidus genome encodes all essential beta-oxidation enzymes, with corresponding genes exhibiting high expression levels—the average fragments per kilobase of transcript per million mapped reads (FPKM) values for these genes in the two oleic acid replicates reached 3842 and 6019, respectively (Fig. 4, Supplementary Table 4). Oleic acid (an 18-carbon ω-9 monoenoic acid) degradation involves the highly expressed 2,4-dienoyl-CoA reductase gene (*fad*H) (FPKM >800) to handle the double bond. The gene encoding the long-chain fatty acid transport protein (FadL) was absent from *Ca.* M. sphaerolipidus genome. This absence was also observed in several published bacterial genomes capable of long-chain fatty acid degradation[24-27], implying the use of alternative transport mechanisms.

The *Ca.* M. sphaerolipidus genome contains two continuous operons for methane production: one comprising *mcr*A, *mcr*G, *mcr*C, *mcr*D, and *mcr*B (sum FPKM >25000), and another containing *mtr*H, *mtr*A, *mtr*B, *mtr*C, *mtr*D, and *mtr*E (sum FPKM >11000), both highly expressed (Fig. 4, Supplementary Table 4). Phylogenetic analysis showed that the *Ca.* M. sphaerolipidus McrA protein sequence clusters with other *Ca.* Methanoglobus sequences within the TACK clade (Fig. 5).

The *Ca.* M. sphaerolipidus highly expressed genes of the WLP (average FPKM > 2300), which operated bidirectionally in a substrate-dependent manner (Fig. 4, Supplementary Table 4). During growth on oleic acid, beta-oxidation produces acetyl-CoA, which is converted to methyl-THMPT and carbon dioxide via the reverse reaction of CO dehydrogenase/acetyl-CoA synthase (CODH/ACS). Methyl-THMPT is then reduced to methane by MTR and MCR. Concurrently, some carbon dioxide is assimilated into methyl-THMPT via the methyl branch of the WLP and converted to methane.

Genes of energy conservation and electron transport complexes showed moderate to high expression (average FPKM >1300) (Fig. 4, Supplementary Table 4). The *Ca.* M. sphaerolipidus genome encodes two copies of heterodisulfide reductase (*hdr*D)

genes, which regenerate coenzymes M and B by reducing heterodisulfide (CoM-S-S-CoB). The electrons required for this reduction may originate from two potential pathways. The first pathway involves electron derivation from hydrogen oxidation via the Mvh-Qmo-Hdr complex coupled with menaquinone (MQ) reduction[18]. The alternative pathway reduces F_{420} via the $F_{420}H_2$: quinone oxidoreductase complex (Fqo), contributing to a reduced MQ pool. The reduced MQ is subsequently utilized by the fused HdrD system for CoM-S-S-CoB reduction. The hydrogen is generated via NAD-reducing hydrogenase (HoxHY) using NADH from beta-oxidation. This hydrogen can be used by FrhB to reduce F_{420} and by the Mvh-Qmo-Hdr complex to reduce ferredoxin. The methyl branch of the WLP requires reduced F_{420}, ferredoxin, and NADH to drive carbon dioxide fixation. Additionally, expression of a V-type ATP synthase genes was also detected at high levels (sum FPKM >4800).

Ca. M. sphaerolipidus genome encodes Pyruvate synthase (Por), pyruvate carboxylase (PycAB), an incomplete reductive TCA cycle, phosphoenolpyruvate synthase (Pps), gluconeogenesis enzymes, and several pentose phosphate pathway enzymes, all expressed at varying levels (Fig. 4, Supplementary Table 4), enabling the synthesis of amino acids, carbohydrates, cell wall components, and nucleic acid sugars.

When oleic acid was supplied, only a few low-abundance MAGs (<0.3%) harbored a complete beta-oxidation pathway, and their gene expression was minimal (FPKM <15) (Supplementary Table 2 and Supplementary Table 5), indicating a negligible role in this process. Other methanogens were detected in the cultures (e.g., *Methanothermobacter*[28, 29], *Methanothrix*[30], *Methanomethylicaceae*[7, 9], *Methanomassiliicoccales*[31]), but the abundance of their MAG were low (metagenome <1.5%, metatranscriptome <1.4%). Their *mcr* and *mtr* genes expression levels were at least an order of magnitude lower than those of *Ca.* M. sphaerolipidus (Supplementary Table 2), and none encods a complete beta-oxidation pathway, suggesting minimal contribution to methane production in the oleic acid cultures.

The pathway of methane production from methanol

The *Ca.* M. sphaerolipidus genome encodes only the methanol methyltransferase *mta*ABC, which was highly expressed during growth on methanol (sum FPKM >11000) (Fig. 4c, Supplementary Table 4), indicating methanol metabolism via MtaABC. In contrast, *Ca.* M. sphaerolipidus lacks methylamine methyltransferases (Mtm, Mtb and Mtt), suggesting an inability to utilize methylamines. This metabolic profile differs from that of *Ca.* M. hypatiae, which uses methylamines but not methanol[18].

During growth on methanol, *Ca.* M. sphaerolipidus also highly expressed genes of the WLP (average FPKM >1600) (Fig. 4c, Supplementary Table 4). The Mta converts methanol to methyl-THMPT, which is primarily transformed into methane via MTR and MCR but can also be oxidized to carbon dioxide via the reverse methyl branch of the WLP. The methyl-THMPT and carbon dioxide can be utilized by the CODH/ACS complex to synthesize acetyl-CoA for biosynthesis. Reverse methyl branch of the WLP generates reducing equivalents, including NADH and reduced F_{420}. These electron carriers support hydrogenogenesis and facilitate the reduction of CoM-S-S-CoB via the Mvh-Qmo-Hdr complex coupled with MQ reduction. Additionally, reduced F_{420} is also oxidized by the Fqo complex, contributing to a reduced MQ pool that is utilized by the HdrD for CoM-S-S-CoB reduction. The *Ca.* M. sphaerolipidus also expressed beta-oxidation genes during growth on methanol (average FPKM >2400) (Fig. 4, Supplementary Table 4), potentially for scavenging trace fatty acids from yeast extract in the medium, a phenomenon previously noted in *Ca.* M. hypatiae during methylamine growth[18].

Diverse methanogenic and methanotrophic metabolisms in *Ca.* Methanoglobus

We retrieved 94 *Ca.* Methanoglobus MAGs from databases, all from terrestrial hot springs (Supplementary Table 6). GTDB taxonomy and phylogenomic analysis classified them into 15 species (Fig. S3), six of which contained *mcr* genes (33 genomes total) (Fig. 6). *Ca.* M. sphaerolipidus belongs to species sp030055595 (Fig. 6a); all five genomes of this species are from Tengchong hot springs, four containing *mcr*. In contrast, the methylamine-metabolizing *Ca.* M. hypatiae belongs to species sp004347865, all genomes of which are from Yellowstone National Park, indicating geographic distribution specificity.

Among the 33 *mcr*-containing genomes, we identified five metabolic groups based on substrate utilization genes (Fig. 6b): 1) seventeen genomes contain both beta-oxidation and methyltransferase genes, suggesting dual capability for fatty acid-driven and methyl-driven methanogenesis, similar to *Ca.* M. sphaerolipidus; 2) four genomes contain beta-oxidation genes but lack methyltransferases, suggesting fatty acid utilization without methyl-based methanogenesis, they may also perform hydrogenotrophic or acetoclastic methanogenesis via the complete WLP; 3) six genomes contain only methyltransferase genes (*mta*, *mtb*, *mtm*, or *mtt*) but lack a complete beta-oxidation pathway, indicating methyl-based methanogenesis; 4) five genomes lack both beta-oxidation and methyltransferase genes and may perform

hydrogenotrophic or acetoclastic methanogenesis; 5) one genome contains sulfate reduction genes (dissimilatory sulfite reductase, *dsr*AB; adenylylsulfate reductase, *apr*AB and sulfate adenylyltransferase, *sat*), suggesting potential for coupling anaerobic methane oxidation with sulfate reduction[21]. These results demonstrate diverse methanogenic and methanotrophic metabolisms within *Ca.* Methanoglobus. Additionally, key enzymatic complexes for energy metabolism—such as the Mvh-Qmo-Hdr complex, HoxHY, the Fqo complex, and the V-type ATP synthase—are relatively conserved across *mcr*-carrying *Ca.* Methanoglobus genomes (Fig. 6b).

Conclusion

Long-chain fatty acids are ubiquitous on Earth[32, 33]. Oleic acid, used here, is a major fatty acid in terrestrial plants and marine phytoplankton[33, 34]. In environments lacking electron acceptors, it has been demonstrated that long-chain fatty acids could be degraded to methane via syntrophic interactions between fermentative bacteria and methanogens[26, 35-37]. Here, our study demonstrates that a single archaeon can directly degrade long-chain fatty acids to produce methane. We propose the term liparotrophy for this process, representing a novel methanogenic mode that expands the known substrate range beyond CO_2 reduction, methylotrophy, acetoclastic methanogenesis, methyl reduction, methoxydotrophy, and alkylotrophy.

Materials and Methods

Etymology

Sphaerolipidus: Gr. fem. n. sphaîra, a ball, sphere; Gr. neut. n. lipos, fatty acid; N.L. masc. n. sphaerolipidus, a spherical archaeon utilizing fatty acid.

Sample collection and cultivation

Sediment samples were collected from a hot spring in Tengchong, China (25.04233°N, 98.82350°E) in January 2020 as described[15]. Site water temperature was 65.7°C and pH 6.7. Sediments were stored in anaerobic bottles under N_2 at room temperature.

Basal mineral medium contained (per liter): 0.5 g NaCl; 0.5 g $MgCl_2 \cdot 6H_2O$; 0.1 g $CaCl_2 \cdot 2H_2O$; 0.3 g NH_4Cl; 0.2 g KH_2PO_4; 0.5 g KCl; 0.4 g $Na_2SO_4 \cdot 7H_2O$; 2.38 g HEPES; 0.1 g yeast extract, autoclaved (121°C, 20 min). Medium was supplemented with 1 mL trace element solution, 1 mL Selenite-Tungstate solution, 1 mL vitamin mix,

1 mL vitamin B1, 1 mL vitamin B12, 0.0005% (w/v) resazurin, 10 mg coenzyme M, 50 mg/L streptomycin, 50 mg/L vancomycin, 1 mM $Na_2S \cdot 9H_2O$; pH adjusted to 7.0 with 2 M NaOH.

Sediments were washed twice with medium by centrifugation (8000 × g, 10 min) in an anaerobic chamber, then resuspended in anaerobic artificial freshwater medium. 110 mL slurries (liquid : sediment ~10:1) were dispensed into 156 mL serum bottles sealed with butyl rubber stoppers (Bellco Glass) and aluminum caps. Oleic acid (500 μL) was added to two experimental bottles, while two additional bottles without oleic acid supplementation served as negative controls (Fig. S1). Incubation began at 60°C in July 2024 (Fig. 1a). Methane production and headspace pressure increased in oleic acid-amended bottles. On day 106, headspace gas was replaced with N_2 to prevent overpressure. On day 159, 200 μL oleic acid was added, and headspace was flushed with N_2. Methane content was monitored until day 238, when 20 mL samples were collected for metagenomic sequencing.

In subsequent subculturing attempts, the cultures were transferred to new bottles with 1-2 volumes of fresh medium and oleic acid as substrate; however, no methane production was detected after transfer. Therefore, the original two bottles were used for all subsequent oleic acid-based incubations (Fig. 2a). For the initial amendment, 100 μL of unlabeled oleic acid was introduced into the 110 mL cultures. After 40 days of incubation, 20% of the culture volume was replaced with fresh medium, the headspace was purged with nitrogen, and 100 μL of ^{13}C-labeled oleic acid was added. Following another 40 days of incubation, 20% of the culture volume was again replaced with fresh medium, the headspace was purged with nitrogen, and 100 μL of unlabeled oleic acid was added. After 19 days of incubation, samples were collected for metagenomic and metatranscriptomic sequencing.

Although transferring the cultures to new bottles with oleic acid did not result in detectable methane production, methane production was observed when methanol was added. From each of the two oleic acid enrichment bottles (Fig. 3a), 20 mL of culture was collected, mixed, and evenly distributed into two new bottles. Each new bottle was supplemented with 40 mL of fresh medium, resulting in a total volume of 60 mL, along with 72.9 μL (30mM) of unlabeled methanol. After 40 days of incubation, 20% of the culture volume was replaced with fresh medium, the headspace was purged with nitrogen, and 72.9 μL of ^{13}C-labeled methanol was added. Following another 40 days of incubation, 20% of the culture volume was again replaced with fresh medium, the

headspace was purged with nitrogen, and 72.9 µL of unlabeled methanol was added. After 16 days of incubation, samples were collected for metagenomic and metatranscriptomic sequencing.

Metagenomic and metatranscriptomic sequencing

Total DNA was extracted using FastDNA® Spin Kit for Soil (MPBIO, USA). Libraries were prepared with Hyper Prep Kit (KAPA, USA) with index codes. Total RNA was extracted using RNA PowerSoil® Total RNA Isolation Kit (Qiagen, Germany). Reverse transcription and mRNA-seq libraries were generated with TruSeq Stranded mRNA LT Sample Prep Kit (Illumina, USA). Libraries were sequenced on GBI-T7 (BGI, China; metagenome) and Illumina Novaseq6000 (Illumina, USA; metatranscriptome) platforms at Personal Biotechnology Co., Ltd. (China).

Metagenomic assembly, binning, and annotation

Reads were trimmed with Trimmomatic (v0.39)[38]. Dereplicated, trimmed paired-end reads were assembled with Megahit (v1.2.9)[39]. Open reading frames (ORFs) on contigs >1 kb were predicted with Prodigal (v2.6.3; -p meta)[40]. Clean reads were mapped to contigs with Bowtie2 (v2.2.8; --very-sensitive)[41]. Contigs >1 kb were binned with MaxBin (v2.2.4)[42]. Genome completeness and contamination were assessed with CheckM (v1.1.3)[43]. MAGs were classified using GTDB (https://gtdb.ecogenomic.org/)[44] and annotated with eggnog-mapper-1.03 (EggNOG; e-value 10^{-10}). Pathway completeness was assessed using KEGG (www.kegg.jp). MAG abundances were calculated with CoverM (v0.6.1; https://github.com/wwood/CoverM).

Metatranscriptomic analysis

Reads were filtered with fastp (v0.20.0). rRNA reads were removed with bbduk (v39.06) against the SILVA SSU138 database (https://www.arb-silva.de/). Filtered reads were mapped to metagenomic contigs with Bowtie2 (v2.2.8; --very-sensitive)[41]. Gene expression (FPKM) was estimated with Cufflinks (v2.2.1; http://cole-trapnell-lab.github.io/cufflinks/). MAG transcriptomic abundances were calculated with CoverM.

Phylogenetic analyses

A phylogenomic tree was constructed from 37 conserved marker genes[21, 45] using MAFFT (v7.313; --ep 0 --genafpair --maxiterate 1000)[46] for alignment, trimAl (v1.4.rev2; -automated1)[47] for filtering, and IQ-Tree (v1.6.6; model LG + C60 + F + G; 1000 bootstraps) [48] for tree building. For the phylogenetic analysis of functional marker proteins (AcrA and McrA), the respective protein sequences were retrieved from the

MAGs, and additional reference sequences were obtained from the NCBI (https://www.ncbi.nlm.nih.gov/protein/). Alignment, filtering and tree building were carried out with the same programs described above. iTOL (http://itol.embl.de/) was used to modify the phylogenetic trees.

***Ca.* M. sphaerolipidus-specific 16S rRNA primer design**

The 16S rRNA gene was extracted from MAGs of *Ca.* M. sphaerolipidus. Six highly similar (>97%) sequences (KP784730.1, FJ638508.1, FJ638514.1, GU179414.1, FJ638504.1, FJ638520.1, FJ638519.1, FJ638518.1, FJ638521.1, FJ638522.1, FJ638523.1, KT453573.1) were downloaded from NCBI. Homologous sequences were aligned with ClustalX[49], probe sequences were selected from aligned regions: Sphaero-910, 5'-GCTTCCCAGCGTTGAATCTAAT-3'. Its specificity was tested using TestProbe 3.0 in the Silva 138 database.

HCR-FISH

Culture samples (1 ml) were fixed in 1% formaldehyde for 12 h at 4 °C. The fixed samples were filtered onto GTTP polycarbonate filter (0.2 μM pore size; Millipore, Darmstadt, Germany) and washed twice with 5 ml 1× PBS, then stored at -20 °C. HCR-FISH was carried out as previously described[50]. A universal Archaea-specific probe ARC915[51], Bacteria-specific probe EUB338[52] and *Ca.* M. sphaerolipidus specific probe Sphaero-910 were used in this study. Hybridization of probe Sphaero-910 occurred at 46 °C with 25% formamide (v/v).

Concentration and carbon isotopic measurement of methane and carbon dioxide

Methane was quantified (data are shown in Fig. 1a) by gas chromatography (Agilent 8890 GC) using a flame ionization detector (FID) with a DB-1 (2 m × 0.25 mm × 0.25μm) filling column. The detection conditions were 60 °C at the inlet, 40 °C at the column temperature, 300 °C at the detector, 99.999% nitrogen gas as carrier gas, 1 ml/min at the flow rate. Methane and carbon dioxide (data are shown in Fig. 2a and Fig. 3a) were quantified by gas chromatography (Shimadzu GC-14B) using a flame ionization detector (FID) with a TDX-02 (2 m × 2 mm) filling column. The detection conditions were 100 °C at the inlet, 100 °C at the column temperature, 250 °C at the detector, 99.999% argon gas as carrier gas, 30 ml/min at the flow rate, and 380 °C at the methane reformer.

The carbon isotope composition of methane and carbon dioxide were analyzed by GasBench II/PreCon-Isotope Ratio Mass Spectrometry (GB/PreCon-IRMS) 253 plus.

Carbon dioxide gas samples are directly introduced into IRMS through GasBench. Methane is converted to carbon dioxide under high-temperature conditions (1000 °C) using Precon, pre-concentrated, and then introduced into IRMS for measurement.

Gibbs free energy calculation

Gibbs free energy values was calculated using eQuilibrator (https://equilibrator.weizmann.ac.il/).

Data availability

The rawdata of metagenome and metatranscriptome have also been deposited in NODE (The National Omics Data Encyclopedia, https://www.biosino.org/node) under accession numbers OEP00006641.

References

1. Saunois, M. et al. The Global Methane Budget 2000–2017. *Earth System Science Data* **12**, 1561-1623 (2020).
2. Conrad, R. The global methane cycle: recent advances in understanding the microbial processes involved. *Environ. Microbiol. Rep.* **1**, 285-92 (2009).
3. Garcia, P. S. et al. Diversity and Evolution of Methane-Related Pathways in Archaea. *Annu. Rev. Microbiol.* **76**, 727-755 (2022).
4. Mayumi, D. et al. Methane production from coal by a single methanogen. *Science* **354**, 222-225 (2016).
5. Zhou, Z. et al. Non-syntrophic methanogenic hydrocarbon degradation by an archaeal species. *Nature* **601**, 257-262 (2022).
6. Kohtz, A. J. et al. Cultivation of *Methanonezhaarchaeia*, the third class of methanogens within the phylum *Thermoproteota*. *bioRxiv*, 2025.06.25.661132 (2025).
7. Kohtz, A. J. et al. Cultivation and visualization of a methanogen of the phylum *Thermoproteota*. *Nature* **632**, 1118-1123 (2024).
8. Krukenberg, V. et al. Methyl-reducing methanogenesis by a thermophilic culture of *Korarchaeia*. *Nature* **632**, 1131-1136 (2024).
9. Wu, K. et al. Author Correction: Isolation of a methyl-reducing methanogen outside the *Euryarchaeota*. *Nature* **633**, E3 (2024).

10. Scheller, S. et al. The key nickel enzyme of methanogenesis catalyses the anaerobic oxidation of methane. *Nature* **465**, 606-608 (2010).

11. Laso-Pérez, R. et al. Thermophilic archaea activate butane via alkyl-coenzyme M formation. *Nature* **539**, 396-401 (2016).

12. Benito Merino, D. et al. Anaerobic hexadecane degradation by a thermophilic *Hadarchaeon* from Guaymas Basin. *ISME J.* **18**, wrad004 (2024).

13. Chen, S. C. et al. Anaerobic oxidation of ethane by archaea from a marine hydrocarbon seep. *Nature* **568**, 108-111 (2019).

14. Zehnle, H. et al. *Candidatus* Alkanophaga archaea from Guaymas Basin hydrothermal vent sediment oxidize petroleum alkanes. *Nat. Microbiol.* **8**, 1199-1212 (2023).

15. Yu, T. et al. Author Correction: Thermophilic *Hadarchaeota* grow on long-chain alkanes in syntrophy with methanogens. *Nat. Commun.* **16**, 412 (2025).

16. Wang, Y. et al. Methyl/alkyl-coenzyme M reductase-based anaerobic alkane oxidation in archaea. *Environ. Microbiol.* **23**, 530-541 (2020).

17. Wang, Y. Z. et al. A methylotrophic origin of methanogenesis and early divergence of anaerobic multicarbon alkane metabolism. *Sci. Adv.* **7**, eabd7180 (2021).

18. Lynes, M. M. et al. Methylotrophic methanogenesis in the *Archaeoglobi* revealed by cultivation of *Ca.* Methanoglobus hypatiae from a Yellowstone hot spring. *ISME J* **18**, wrae026 (2024).

19. Wang, J. et al. Evidence for nontraditional mcr-containing archaea contributing to biological methanogenesis in geothermal springs. *Sci. Adv.* **9**, eadg6004 (2023).

20. Buessecker, S. et al. Mcr-dependent methanogenesis in *Archaeoglobaceae* enriched from a terrestrial hot spring. *ISME J* **17**, 1649-1659 (2023).

21. Wang, Y. et al. Expanding anaerobic alkane metabolism in the domain of Archaea. *Nat. Microbiol.* **4**, 595-602 (2019).

22. Slobodkina, G. et al. Physiological and Genomic Characterization of a Hyperthermophilic Archaeon *Archaeoglobus neptunius* sp. nov. Isolated From a Deep-Sea Hydrothermal Vent Warrants the Reclassification of the Genus *Archaeoglobus*. *Front. Microbiol.* **12**, 679245 (2021).

23. Mori, K. et al. *Archaeoglobus infectus* sp. nov., a novel thermophilic, chemolithoheterotrophic archaeon isolated from a deep-sea rock collected at Suiyo Seamount, Izu-Bonin Arc, western Pacific Ocean. *Int. J. Syst. Evol. Microbiol.* **58**, 810-816 (2008).

24. Pérez-Bernal, M. F. et al. *Desulfobotulus mexicanus* sp. nov., a novel sulfate-reducing bacterium isolated from the sediment of an alkaline crater lake in Mexico. *Int. J. Syst. Evol. Microbiol.* **70**, 3219-3225 (2020).

25. Wu, C. et al. *Syntrophomonas wolfei* subsp. *methylbutyratica* subsp. nov., and assignment of *Syntrophomonas wolfei* subsp. *saponavida* to *Syntrophomonas saponavida* sp. nov. comb. nov. *Syst. Appl. Microbiol.* **30**, 376-80 (2007).

26. Sousa, D. Z. et al. *Syntrophomonas zehnderi* sp. nov., an anaerobe that degrades long-chain fatty acids in co-culture with *Methanobacterium formicicum*. *Int. J. Syst. Evol. Microbiol.* **57**, 609-615 (2007).

27. Hatamoto, M. et al. *Syntrophomonas palmitatica* sp. nov., an anaerobic, syntrophic, long-chain fatty-acid-oxidizing bacterium isolated from methanogenic sludge. *Int. J. Syst. Evol. Microbiol.* **57**, 2137-2142 (2007).

28. Cheng, L. et al. Isolation and characterization of *Methanothermobacter* crinale sp. nov., a novel hydrogenotrophic methanogen from the Shengli oil field. *Appl. Environ. Microbiol.* **77**, 5212-5219 (2011).

29. Nakamura, K. et al. *Methanothermobacter tenebrarum* sp. nov., a hydrogenotrophic, thermophilic methanogen isolated from gas-associated formation water of a natural gas field. *Int. J. Syst. Evol. Microbiol.* **63**, 715-722 (2013).

30. Kamagata, Y. et al. Characterization of three thermophilic strains of *Methanothrix* ("*Methanosaeta*") thermophila sp. nov. and rejection of *Methanothrix* ("*Methanosaeta*") thermoacetophila. *Int. J. Syst. Bacteriol.* **42**, 463-468 (1992).

31. Iino, T. et al. *Candidatus* Methanogranum caenicola: a novel methanogen from the anaerobic digested sludge, and proposal of *Methanomassiliicoccaceae* fam. nov. and *Methanomassiliicoccales* ord. nov., for a methanogenic lineage of the class *Thermoplasmata*. *Microbes. Environ.* **28**, 244-250 (2013).

32. Killops, S., & Killops, V. An Introduction to Organic Geochemistry (2nd ed.).

Blackwell Publishing, (2005).

33. Volkman, J. K. et al. Microalgal biomarkers: A review of recent research developments. *Organic Geochemistry* **29**, 1163-1179 (1998).

34. Li-Beisson, Y., et al. Acyl-lipid metabolism. *The Arabidopsis Book* **11**, e0161 (2013).

35. Fang, B. et al. Enhancing methanogenesis from long-chain fatty acids (LCFA) and enrichment of novel bacteria with resuscitation-promoting factors. *Bioresour. Technol.* **432**, 132663 (2025).

36. Liu, Y. et al. Biokinetic and microbial insights into regulatory mechanisms of long-chain fatty acid degradation during food waste-lipid co-digestion within anaerobic membrane bioreactor. *Bioresour. Technol.* **408**, 131223 (2024).

37. Song, L. et al. Methanogenic degradation of long-chain fatty acids associated with syntrophic microbial dynamics during thermophilic AnMBR treatment of lipid-rich dairy wastes. *Chemical Engineering Journal* **498**, 155702 (2024).

38. Bolger, A. M. et al. Trimmomatic: a flexible trimmer for Illumina sequence data. *Bioinformatics* **30**, 2114-2120 (2014).

39. Li, D. et al. MEGAHIT: an ultra-fast single-node solution for large and complex metagenomics assembly via succinct de Bruijn graph. *Bioinformatics* **31**, 1674-1676 (2015).

40. Hyatt, D. et al. Prodigal: prokaryotic gene recognition and translation initiation site identification. *BMC Bioinformatics* **11**, 119 (2010).

41. Langmead, B. & Salzberg, S. L. Fast gapped-read alignment with Bowtie 2. *Nat. Methods* **9**, 357-359 (2012).

42. Wu, Y. et al. MaxBin 2.0: an automated binning algorithm to recover genomes from multiple metagenomic datasets. *Bioinformatics* **32**, 605-607 (2016).

43. Parks, D. H. et al. CheckM: assessing the quality of microbial genomes recovered from isolates, single cells, and metagenomes. *Genome Research* **25**, 1043-1055 (2015).

44. Parks, D. H. et al. GTDB: an ongoing census of bacterial and archaeal diversity through a phylogenetically consistent, rank normalized and complete genome-based taxonomy. *Nucleic Acids Res.* **50**, D785-D794 (2022).

45. Hug, L. A. et al. A new view of the tree of life. *Nat. Microbiol.* **1**, 16048 (2016).

46. Katoh, K. & Standley, D. M. MAFFT multiple sequence alignment software version 7: improvements in performance and usability. *Mol. Biol. Evol.* **30**, 772-80 (2013).

47. Capella-Gutiérrez, S. et al. trimAl: a tool for automated alignment trimming in large-scale phylogenetic analyses. *Bioinformatics* **25**, 1972-1973 (2009).

48. Nguyen, L. T. et al. IQ-TREE: a fast and effective stochastic algorithm for estimating maximum-likelihood phylogenies. *Mol. Biol. Evol.* **32**, 268-274 (2015).

49. Larkin, M. A. et al. Clustal W and Clustal X version 2.0. *Bioinformatics* **23**, 2947-2948 (2007).

50. Jia, Z. et al. Optimizing the hybridization chain reaction-fluorescence in situ hybridization (HCR-FISH) protocol for detection of microbes in sediments. *Mar. Life Sci. Tech.* **3**, 529-541 (2021).

51. Amann, R. I. et al. Fluorescent-oligonucleotide probing of whole cells for determinative, phylogenetic, and environmental studies in microbiology. *J. Bacteriol.* **172**, 762-770 (1990).

52. Amann, R. I. et al. Combination of 16S rRNA-targeted oligonucleotide probes with flow cytometry for analyzing mixed microbial populations. *Appl. Environ. Microbiol.* **56**, 1919-1925 (1990).

Acknowledgements

We thank Yue Yi (Biogas Institute of Ministry of Agriculture and Rural Affairs) for kind suggestions to improve the manuscript; Qian Luo (School of Life Sciences and Biotechnology, Shanghai Jiao Tong University) and Lili Feng (School of Environmental Science and Engineering, Shanghai Jiao Tong University) for assisting in detection of methane and carbon dioxide; Fan Yang (Instrumental Analysis Center, Shanghai Jiao Tong University) for assisting in detection of carbon isotope composition of methane and carbon dioxide. This work was supported financially by the National Natural Science Foundation of China Grant (42230401, 42276139) to FW and TY, Shanghai Jiao Tong University 2030 initiative (Grant WH510244001) to FW, Science

and Technology Innovation Action Plan Of Shanghai Science and Technology Commission of Shanghai Municipality (24HC2810200) to FW. Global Subseafloor Ecosystem and Sustainability (GSES) and the project 'Ocean Negative Carbon Emission (ONCE)'.

Authors' contributions

TY and FW designed research. TY collected samples; performed culture experiments; designed HCR-FISH probes and performed HCR-FISH; isolated nucleic acid; detected methane and carbon dioxide; analyzed of metagenomic and metatranscriptomic data. SY constructed phylogenetic trees. TY wrote the initial draft, TY, FW and YW reviewed the manuscript.

Competing interests

The authors declare that they have no competing interests.

Figure legends

Figure 1 Methane production and microbial composition of enrichment cultures from hot spring sediments incubated with and without oleic acid. a, Methane accumulation in the headspace of cultures over 238 days. See Supplementary Table 1 for details. **b,** Relative abundance of *Ca.* M. sphaerolipidus in the before incubation slurry and in enrichments after 238 days of incubation, as determined by metagenomic sequencing (MG). Other, including the unmapped reads and MAGs with relative abundance < 5%. See Supplementary Table 2 for details. r1 and r2 represent two replicates. **c,** HCR-FISH analysis of the enrichment culture. Cells were hybridized with probes: Arc915 (targeting archaea, green), a specific probe Sphaero-910 (targeting *Ca.* M. sphaerolipidus, green), and EUB338 (targeting bacteria, red). Subsequently, all cells were counterstained with 4',6-Diamidino-2-Phenylindole (DAPI, blue). Scale bar, 2 μm. **d,** Cell morphology in the enrichment culture as observed by transmission electron microscopy (TEM). Scale bar, 2 μm.

Figure 2 Methane production and community composition of the methanogenic

enrichment cultures containing *Ca.* M. sphaerolipidus with oleic acid as the substrate. a, methane and carbon dioxide content, and ^{13}C-labled methane and carbon dioxide content in the cultures amended with ^{12}C-oleic acid or ^{13}C-oleic acid. See Supplementary Table 1 for details. **b,** community composition of the culture based on the relative abundance of the *Ca.* M. sphaerolipidus genome and other MAGs recovered from metagenomic and metatranscriptomic sequencing (MG+MT). Other, including the unmapped reads and MAGs with relative abundance < 5%. r1 and r2 represent two replicates. See Supplementary Table 2 for details.

Figure 3 Methane production and community composition of the methanogenic enrichment cultures containing *Ca.* M. sphaerolipidus with methanol as the substrate. a, methane and carbon dioxide content, and ^{13}C-labled methane and carbon dioxide content in the cultures amended with ^{12}C-methanol or ^{13}C-methanol. See Supplementary Table 1 for details. **b,** community composition of the culture based on the relative abundance of the *Ca.* M. sphaerolipidus genome and other MAGs recovered from metagenomic and metatranscriptomic sequencing (MG+MT). Other, including the unmapped reads and MAGs with relative abundance < 5%. r1 and r2 represent two replicates. See Supplementary Table 2 for details.

Figure 4 Metabolic model of *Ca.* M. sphaerolipidus. a, genome-inferred model for oleic acid degradation and methane production. **b,** genome-inferred model for methanol degradation and methane production. The names of genes not found in the genome were shown in brown font. Fd_{red}, reduced ferredoxins; Fd_{ox}, oxidized ferredoxins. **c,** Gene expression of *Ca.* M. sphaerolipidus during growth on oleic acid and methanol; for enzymes comprising multiple subunits, the sum of FPKM value representing the transcribed enzymes is used. The dots represent significant differences in gene expression levels were observed (p value <0.05; t-test). The steps involving beta-oxidation, WLP, methanogenesis, methyltransferase, energy metabolism, gluconeogenesis, Pentose Phosphate Pathway (PPP) and TCA cycle. List of related genes and gene transcription levels was showed in Supplementary Table 4.

Figure 5 Phylogenomic affiliation of the AcrAs and McrAs. a, the tree branches were classified into three distinct groups: conventional MCR clade, the TACK clade, and the

ACR clade. **b,** shows MAGs of genus *Ca.* Methanoglobus. Maximum-likelihood tree, alignments were generated using MAFFT[46] and then filtered with trimAl[47], and the trees were built by the IQ-Tree[48] method with the model LG + C60 + F + G with 1,000 bootstrap replicates. Bootstrap values >90% shown in black dots.

Figure 6 Phylogenomic affiliation and proposed methane production pathway of *mcr*-carrying MAGs in genus *Ca.* Methanoglobus. a, phylogenomic affiliation of the *Ca.* Methanoglobus MAGs based on 37 conserved protein sequences and using 107 representative archaeal genomes. Maximum-likelihood tree, alignments were generated using MAFFT[46] and then filtered with trimAl[47], and the trees were built by the IQ-Tree[48] method with the model LG + C60 + F + G with 1,000 bootstrap replicates. Bootstrap values >90% shown in black dots. The *mcr*-carrying MAGs shown in red, the number in parentheses following each species identifier indicates the count of *mcr*-carrying MAGs within that species and the total number of MAGs for the species. **b,** proposed methane production pathway of *mcr*-carrying MAGs in genus *Ca.* Methanoglobus. Presence, partial and absence of key metabolic genes and methanogenesis marker proteins. See Supplementary Table 6 for details.

Figures

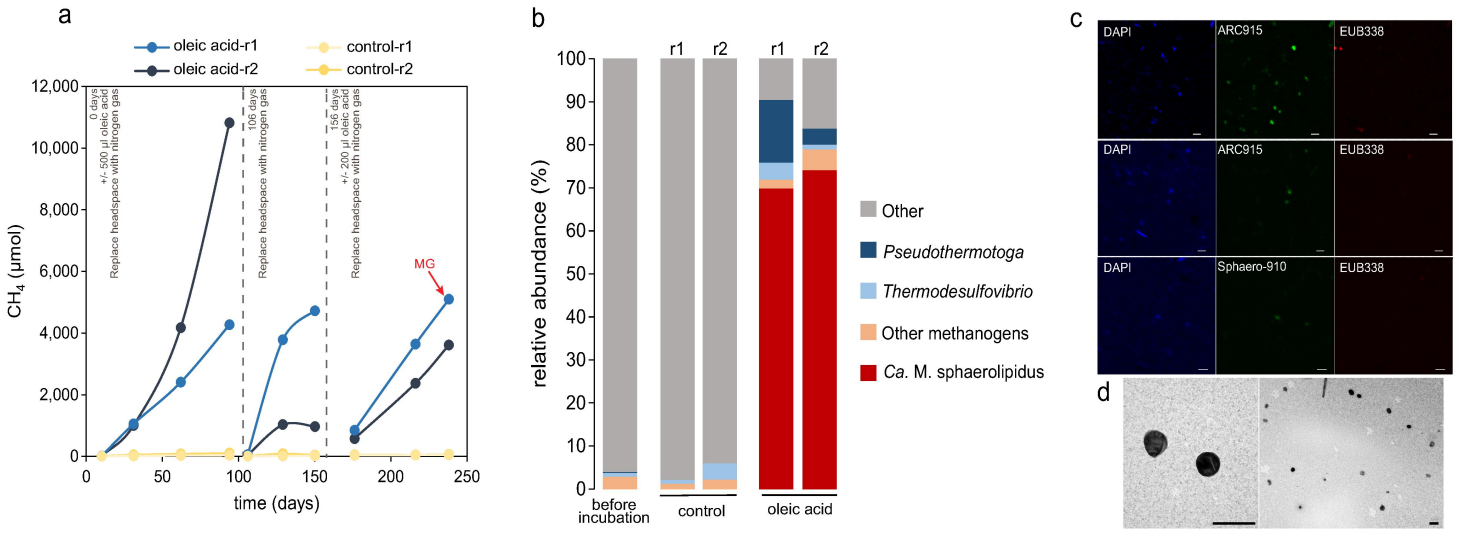


Figure 1

Methane production and microbial composition of enrichment cultures from hot spring sediments incubated with and without oleic acid. a, Methane accumulation in the headspace of cultures over 238 days. See Supplementary Table 1 for details. b, Relative abundance of Ca. M. sphaerolipidus in the before incubation slurry and in enrichments after 238 days of incubation, as determined by metagenomic sequencing (MG). Other, including the unmapped reads and MAGs with relative abundance < 5%. See Supplementary Table 2 for details. r1 and r2 represent two replicates. c, HCR-FISH analysis of the enrichment culture. Cells were hybridized with probes: Arc915 (targeting archaea, green), a specific probe Sphaero-910 (targeting Ca. M. sphaerolipidus, green), and EUB338 (targeting bacteria, red). Subsequently, all cells were counterstained with 4',6-Diamidino-2-Phenylindole (DAPI, blue). Scale bar, 2 µm. d, Cell morphology in the enrichment culture as observed by transmission electron microscopy (TEM). Scale bar, 2 µm.

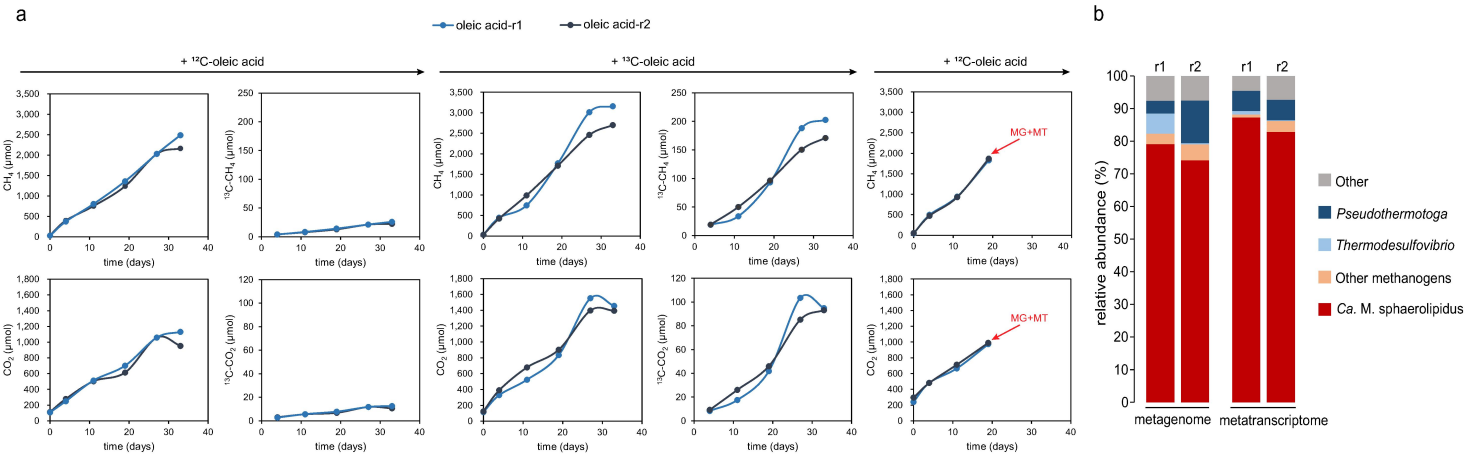


Figure 2

Methane production and community composition of the methanogeni enrichment cultures containing Ca. M. sphaerolipidus with oleic acid as the substrate. a, methane and carbon dioxide content, and 13 C-labled methane and carbon dioxide content in the cultures amended with 12 C-oleic acid or 13 C-oleic acid. See Supplementary Table 1 for details. b, community composition of the culture based on the relative abundance of the Ca. M. sphaerolipidus genome and other MAGs recovered from metagenomic and metatranscriptomic sequencing (MG+MT). Other, including the unmapped reads and MAGs with relative abundance < 5%. r1 and r2 represent two replicates. See Supplementary Table 2 for details.

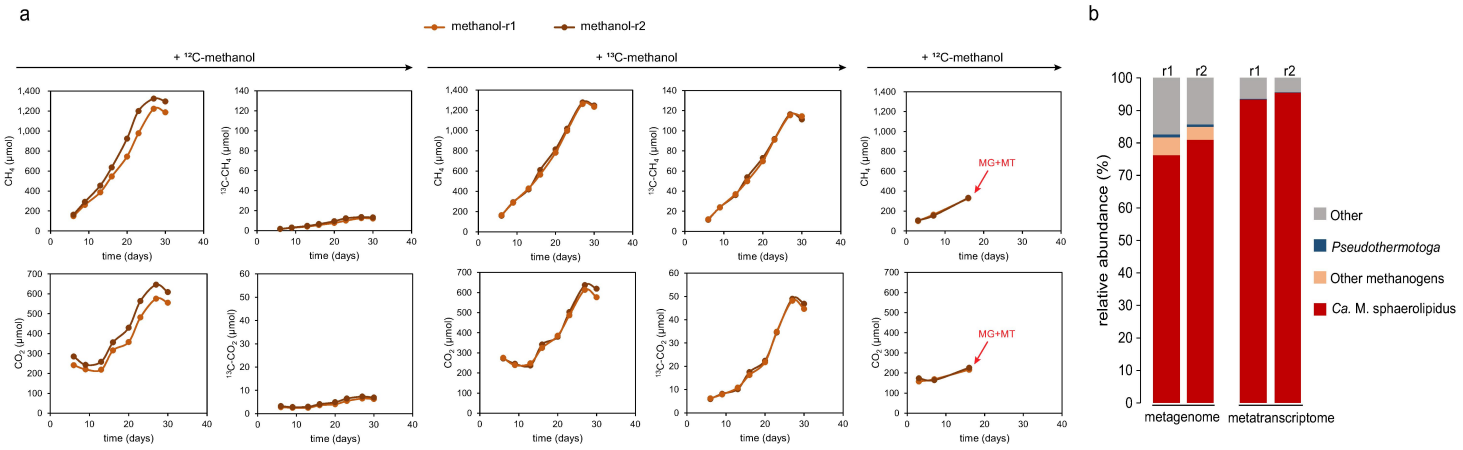


Figure 3

Methane production and community composition of the methanogenic enrichment cultures containing Ca. M. sphaerolipidus with methanol as the substrate. a, methane and carbon dioxide content, and 13 C-labled methane and carbon dioxide content in the cultures amended with 12 C-methanol or 13 C-methanol. See Supplementary Table 1 for details. b, community composition of the culture based on the relative abundance of the Ca. M. sphaerolipidus genome and other MAGs recovered from metagenomic and metatranscriptomic sequencing (MG+MT). Other, including the unmapped reads and MAGs with relative abundance < 5%. r1 and r2 represent two replicates. See Supplementary Table 2 for details.

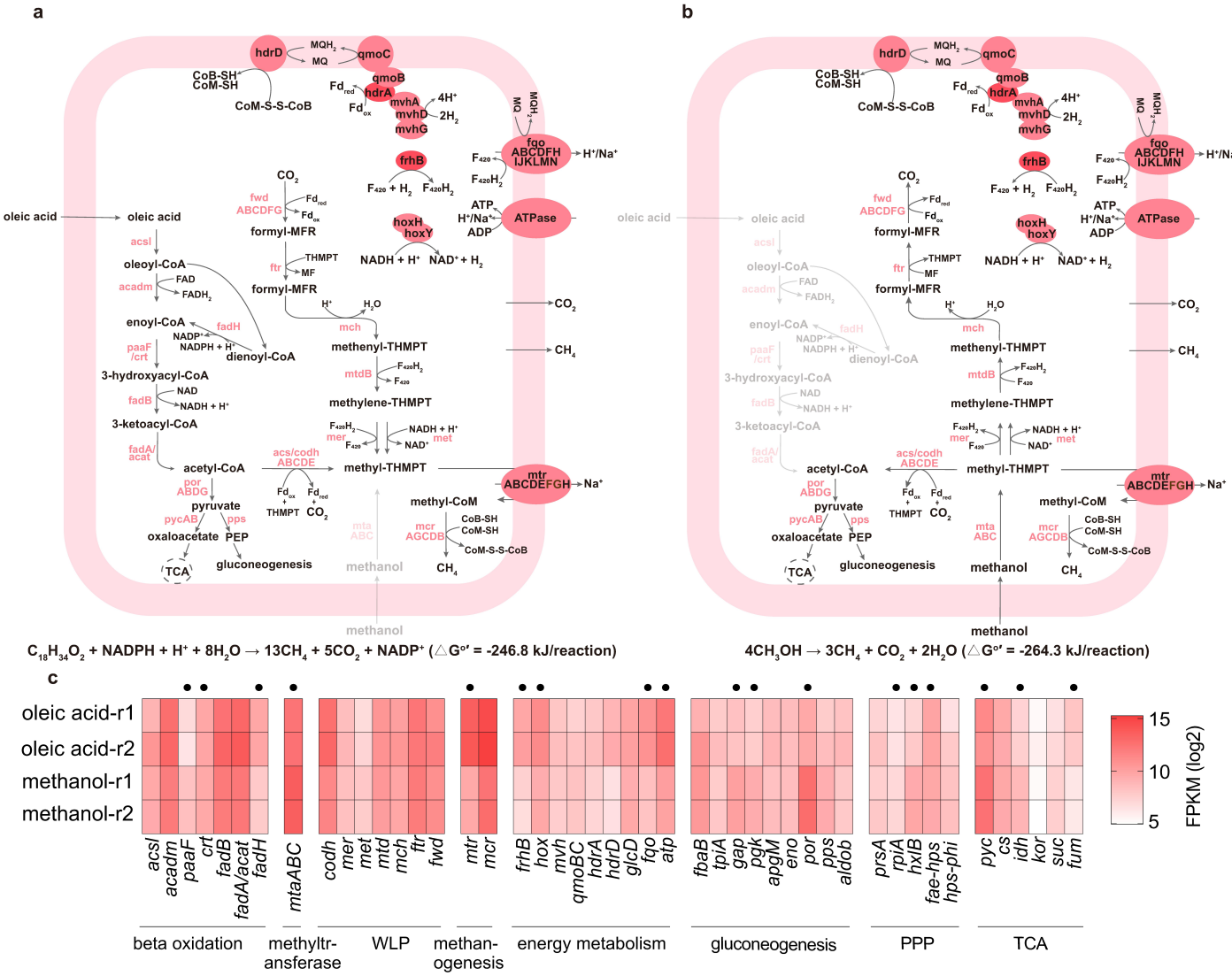


Figure 4

Metabolic model of Ca. M. sphaerolipidus. a, genome-inferred model for oleic acid degradation and methane production. b, genome-inferred model for methanol degradation and methane production. The names of genes not found in the genome were shown in brown font. Fdred, reduced ferredoxins; Fdox, oxidized ferredoxins. c, Gene expression of Ca. M. sphaerolipidus during growth on oleic acid and methanol; for enzymes comprising multiple subunits, the sum of FPKM value representing the transcribed enzymes is used. The dots represent significant differences in gene expression levels were observed (p value <0.05; t-test). The steps involving beta- oxidation, WLP, methanogenesis, methyltransferase, energy metabolism, gluconeogenesis, Pentose Phosphate Pathway (PPP) and TCA cycle. List of related genes and gene transcription levels was showed in Supplementary Table 4.

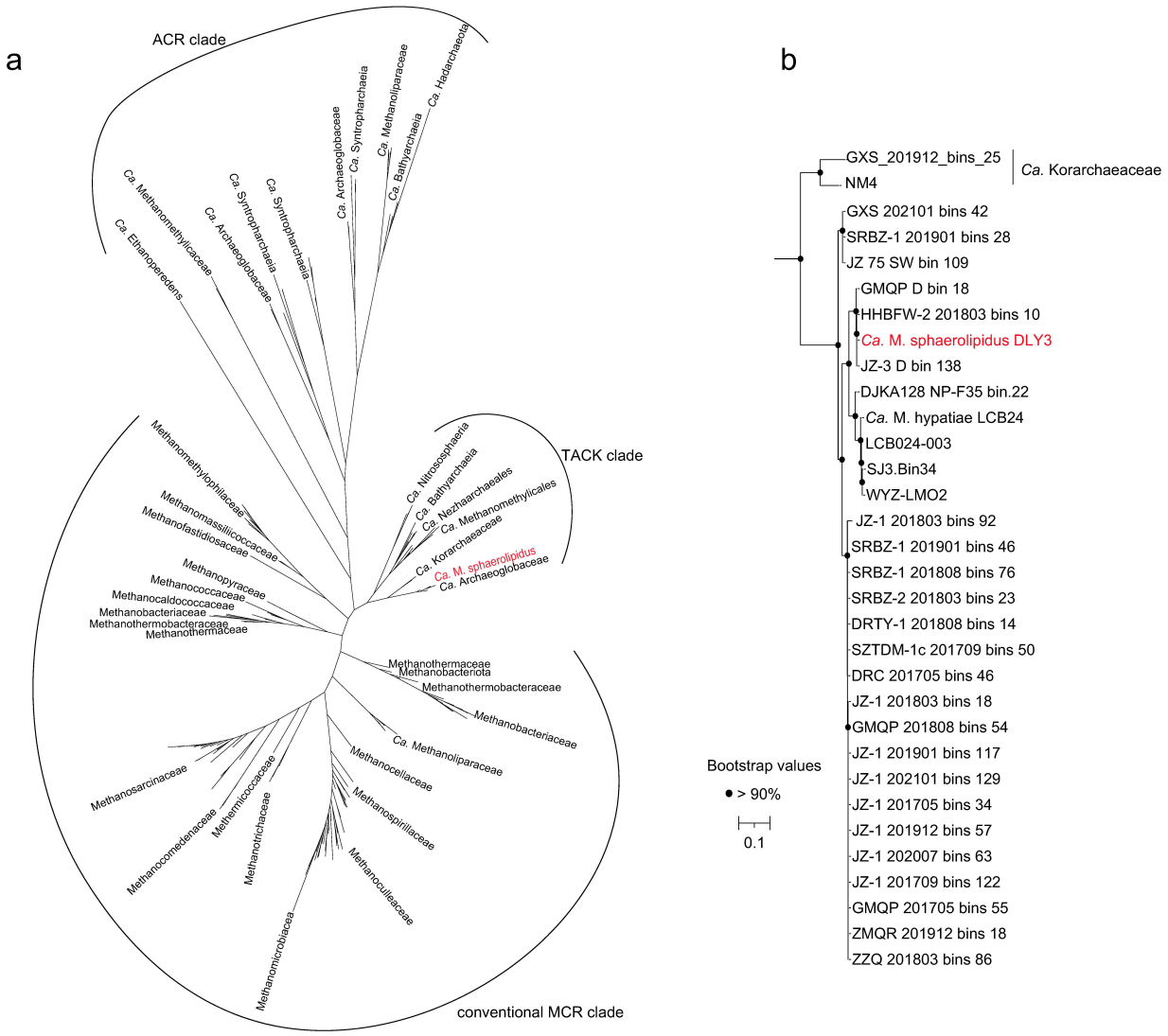


Figure 5

Phylogenomic affiliation of the AcrAs and McrAs. a, the tree branches were classified into three distinct groups: conventional MCR clade, the TACK clade, and the ACR clade. b, shows MAGs of genus Ca. Methanoglobus. Maximum-likelihood tree, alignments were generated using MAFFT46 and then filtered with trimAl47 , and the trees were built by the IQ-Tree48 method with the model LG + C60 + F + G with 1,000 bootstrap replicates. Bootstrap values >90% shown in black dots.

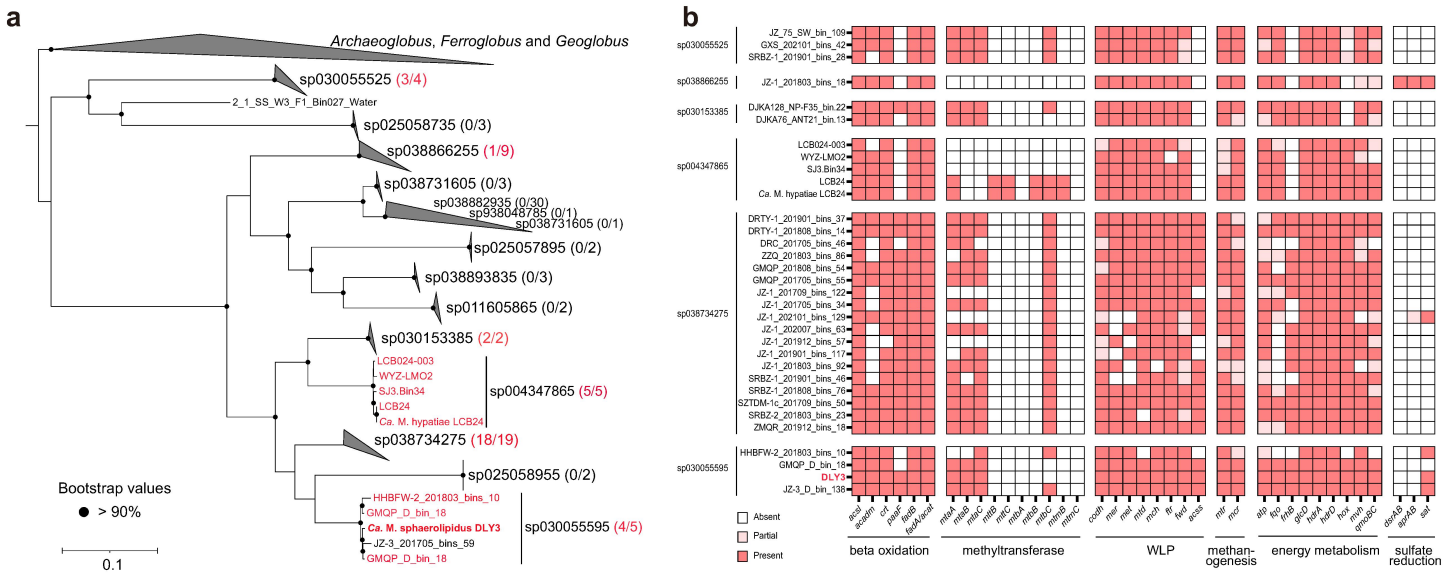


Figure 6

Phylogenomic affiliation and proposed methane production pathway of mcr-carrying MAGs in genus Ca. Methanoglobus. a, phylogenomic affiliation of the Ca. Methanoglobus MAGs based on 37 conserved protein sequences and using 107 representative archaeal genomes. Maximum-likelihood tree, alignments were generated using MAFFT46 and then filtered with trimAl47 , and the trees were built by the IQ- Tree48 method with the model LG + C60 + F + G with 1,000 bootstrap replicates. Bootstrap values >90% shown in black dots. The mcr-carrying MAGs shown in red, the number in parentheses following each species identifier indicates the count of mcr- carrying MAGs within that species and the total number of MAGs for the species. b, proposed methane production pathway of mcr-carrying MAGs in genus Ca. Methanoglobus. Presence, partial and absence of key metabolic genes and methanogenesis marker proteins. See Supplementary Table 6 for details.

Supplementary Files

This is a list of supplementary files associated with this preprint. Click to download.

- SupplementaryTable1.xlsx
- SupplementaryTable2.xlsx
- SupplementaryTable4.xlsx
- SupplementaryTable3.xlsx
- SupplementaryInformation.pdf
- SupplementaryTable5.xlsx
- SupplementaryTable6.xlsx